# Layered hydrogels accelerate iPSC-derived neuronal maturation and reveal migration defects caused by MeCP2 dysfunction

Zhen-Ning Zhang[a], Beatriz C. Freitas[b,c], Hao Qian[d,e], Jacques Lux[a,1], Allan Acab[b,c], Cleber A. Trujillo[b,c], Roberto H. Herai[b,c,2], Viet Anh Nguyen Huu[a], Jessica H. Wen[f], Shivanjali Joshi-Barr[a], Jerome V. Karpiak[b,c], Adam J. Engler[f,g], Xiang-Dong Fu[d,e], Alysson R. Muotri[b,c,3], and Adah Almutairi[a,3]

[a]Skaggs School of Pharmacy and Pharmaceutical Sciences, University of California, San Diego, La Jolla, CA 92093; [b]Department of Pediatrics, Rady Children's Hospital-San Diego, San Diego, CA 92123; [c]Stem Cell Program, Department of Cellular & Molecular Medicine, University of California, San Diego School of Medicine, Sanford Consortium for Regenerative Medicine, La Jolla, CA 92037; [d]Department of Cellular and Molecular Medicine, University of California, San Diego, La Jolla, CA 92093-0651; [e]Institute of Genomic Medicine, University of California, San Diego, La Jolla, CA 92093-0651; [f]Department of Bioengineering, University of California, San Diego, La Jolla, CA 92093; and [g]Sanford Consortium for Regenerative Medicine, La Jolla, CA 92037

Probing a wide range of cellular phenotypes in neurodevelopmental disorders using patient-derived neural progenitor cells (NPCs) can be facilitated by 3D assays, as 2D systems cannot entirely recapitulate the arrangement of cells in the brain. Here, we developed a previously unidentified 3D migration and differentiation assay in layered hydrogels to examine how these processes are affected in neurodevelopmental disorders, such as Rett syndrome. Our soft 3D system mimics the brain environment and accelerates maturation of neurons from human induced pluripotent stem cell (iPSC)-derived NPCs, yielding electrophysiologically active neurons within just 3 wk. Using this platform, we revealed a genotype-specific effect of methyl-CpG-binding protein-2 (MeCP2) dysfunction on iPSC-derived neuronal migration and maturation (reduced neurite outgrowth and fewer synapses) in 3D layered hydrogels. Thus, this 3D system expands the range of neural phenotypes that can be studied in vitro to include those influenced by physical and mechanical stimuli or requiring specific arrangements of multiple cell types.

3D hydrogels | neuronal migration and maturation | 3D RTT modeling

Neuronal migration and maturation is a key step in brain development. Defects in this process have been implicated in many disorders, including autism (1) and schizophrenia (2). Thoroughly understanding how neural progenitor cell (NPC) migration is affected in neurodevelopmental disorders requires a means of dissecting the process using cells with genetic alterations matching those in patients. Existing in vitro assays of migration generally involve measurement of cell movement across a scratch or gap or through a membrane toward a chemoattractant in 2D culture systems. Although widely used, such assays may not accurately reveal in vivo differences, as neuronal migration is tightly regulated by physical and chemical cues in the extracellular matrix (ECM) that NPCs encounter as they migrate.

In vitro 3D culture systems offer a solution to these limitations (3–7). Compared with 2D culture, a 3D arrangement allows neuronal cells to interact with many more cells (4); this similarity to the in vivo setting has been shown to lengthen viability, enhance survival, and allow formation of longer neurites and more dense networks in primary neurons in uniform matrices or aggregate culture (8, 9). Indeed, 3D culture systems have been used to study nerve regeneration, neuronal and glial development (10–12), and amyloid-β and tau pathology (13). Thus, measuring neuronal migration through a soft 3D matrix would continue this trend toward using 3D systems to study neuronal development and pathology.

We sought to develop a 3D assay to examine potential migration and neuronal maturation defects in Rett syndrome (RTT), a genetic neurodevelopmental disorder that affects 1 in 10,000 children in the United States and is caused by mutations in the

X-linked methyl-CpG-binding protein-2 (*MECP2*) gene (14). Studies using induced pluripotent stem cells (iPSCs) from RTT patients in traditional 2D adherent culture have revealed reduced neurite outgrowth and synapse number, as well as altered calcium transients and spontaneous postsynaptic currents (1). However, 2D migration assays seemed unlikely to reveal inherent defects in this developmental process, which could be affected because MeCP2 regulates multiple developmental related genes (15). Migration of RTT iPSC-derived NPCs has not previously been studied.

Using a previously unidentified 3D tissue culture system that allows creation of layered architectures, we studied differences in migration of MeCP2-mutant iPSC-derived versus control iPSC-derived NPCs. This approach revealed a defect in migration of MeCP2-mutant iPSC-derived NPCs induced by either astrocytes or neurons. Further, this 3D system accelerated maturation of

## Significance

Three-dimensional systems enable the formation of tissue-mimetic architectures and promote more realistic physiological responses than conventional 2D systems. Here we report a previously unidentified layered 3D culture system to assay migration and maturation of human induced pluripotent stem cell (iPSC)-derived neural progenitor cells (NPCs) and reveal a genotype-specific effect of methyl-CpG-binding protein-2 (MeCP2) dysfunction on iPSC-derived neuronal migration and maturation in 3D layered hydrogels. Using this platform, we identified a migration defect in MeCP2-mutant iPSC-derived NPCs and confirmed previous observations that neurons derived from these cells have reduced neurite outgrowth and fewer synapses. Meanwhile, 3D hydrogel culture accelerates neuronal differentiation of iPSC-derived NPCs.

ENGINEERING

neurons from human iPSC-derived NPCs, yielding electrophysiologically active neurons within just 3 wk. With mature neurons derived from RTT patients and controls, we further confirmed defective neurite outgrowth and synaptogenesis in MeCP2-mutant neurons. Thus, this 3D system enables study of morphological features accessible in 2D system as well as previously unexamined phenotypes.

## Results

**Modular Design of Layered Hydrogels for Migration of Human iPSC-Derived NPCs.** We developed a previously unidentified and simple assay measuring migration through a soft 3D matrix to better imitate the physical environment within the brain. This 3D hydrogel-based migration assay relies on density gradient multilayer polymerization (16), which consists simply of mixing small-molecule density modifiers with prepolymer-containing cell suspensions and gently layering them with a syringe. The prepolymer in these studies was methacrylate-modified hyaluronic acid (HAMA, 17 ± 1% methacrylation); varying ultraviolet A (UVA) irradiation

time yielded hydrogels of variable stiffness (Fig. 1 *A* and *B*). Hydrogels with stiffness around 100 Pa and pore size around 10 μm were used (Fig. 1*C*). By recreating cell–cell interactions, 3D layered structures enable the formation of tissue-mimetic architectures and promote more realistic physiological responses than conventional 2D culture. We used the layered hydrogel model to investigate the migration of NPCs toward different neuronal cell types: NPCs, astrocytes, or neurons (Fig. 1*D*). As astrocytes have been shown to promote neural migration (17), we first evaluated NPC migration toward these cells. Human NPCs were derived from human nonaffected control iPSC lines (WT83) and infected with lentivirus expressing green fluorescent protein (GFP) under the control of the cytomegalovirus (CMV) promoter to track migration by microscopy. Immunofluorescence and flow cytometry confirmed expression of progenitor markers Nestin, Sox1, Sox2, and PAX6 (Fig. S1 *A* and *B*). Human astrocytes were generated from differentiated human NPCs and infected with lentivirus expressing tdTomato under the control of the glial fibrillary acidic protein (GFAP) promoter, then enriched by flow cytometry for tdTomato-positive cells (Fig. S1 *C* and *D*). Immunofluorescence confirmed expression of astrocyte markers, GFAP, and S100 calcium-binding protein β (S100β) (Fig. S1*E*). Migration was examined in two-layered hydrogels containing sorted GFAP::tdTomato-positive astrocytes in the top and CMV::GFP-positive NPCs in the bottom layer, cultured in either neuronal growth medium (NG) or astrocyte culture medium (AG), respectively. After 3 d, we observed dramatic NPC migration toward astrocytes (Fig. 1 *E* and *F*). Using real-time fluorescence microscopy, we showed NPC migration toward astrocytes in a time-dependent manner (Fig. 1*G*). To further confirm that NPCs in the bottom layer were migrating toward astrocytes, we used fluorescence-labeled HAMA to identify the top layer in our 3D migration assay. We found that GFAP::tdTomato-positive astrocytes remained in the fluorescence-labeled top layer, whereas CMV::GFP-positive differentiating NPCs migrated into it (Fig. 1*H*).

We further evaluated NPC migration induced by neurons in our 3D system. Human neurons positive for the neuronal markers β-III-tubulin (Tuj1) and Map2 (Fig. S1*F*) were generated from differentiated human NPCs as described (1) and enriched by magnetic-activated cell sorting for CD44 and CD184 double-negative cells (Fig. S1*G*). CD44 and CD184 were cell-surface markers for the isolation of neurons derived from human pluripotent stem cells (18). These neurons were seeded in the top layer, and CMV::tdTomato NPCs were seeded in the bottom layer. We observed NPC migration induced by neurons after 3 d of coculture (Fig. 1 *E* and *F*). On the contrary, when NPCs were seeded in both layers, NPCs in the bottom layer did not migrate (Fig. 1 *E* and *F*). Taken together, this 3D assay measures NPC migration toward either astrocytes or neurons.

**Defective Migration of NPCs Derived from RTT iPSCs.** With this 3D migration system, we sought to examine whether MeCP2 mutations found in RTT patients affect neuronal migration, as MeCP2 regulates multiple genes involved in this process (15). Further, mutations in one of these, cyclin-dependent kinase-like 5 (CDKL5), have been identified in patients with RTT (19); knockdown of CDKL5 in rats causes delayed neuronal migration (20). Despite the current consensus that RTT does not involve migration defects (21), this process may be affected in some RTT-affected individuals.

We compared migration of NPCs derived from RTT patients and their parental controls (1). First, we used NPCs derived from a male RTT patient (Q83X) and his nonaffected father's iPSC lines. Migration was examined in two-layer hydrogels containing sorted GFAP::tdTomato-positive astrocytes in the top layer and CMV::GFP-positive NPCs in the bottom layer. Q83X NPC migration toward Q83X astrocytes was retarded ~70% compared with WT83 NPCs toward WT83 astrocytes, indicating a migration defect (Fig. 2 *A* and *C*). In the meantime, Q83X NPCs migration toward
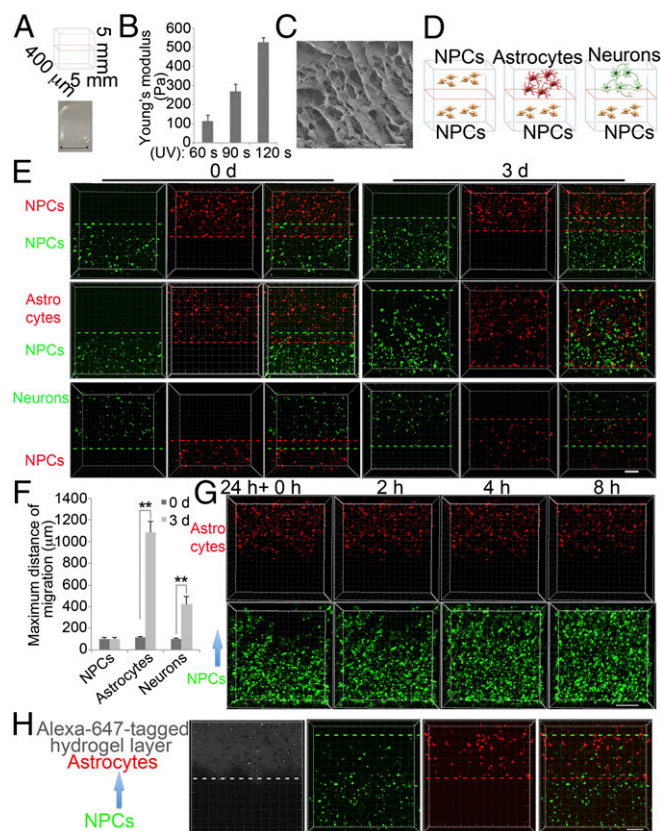


**Fig. 1.** Setup of layered hydrogels to study migration of human iPSC-derived NPCs. (*A*) Bright-field image of two-layered hydrogels. (Scale bar, 5 mm.) (*B*) Compressive moduli of HAMA hydrogels measured by atomic force microscope (AFM) following varying UV exposure time. (*C*) Scanning electron microscopy (SEM) imaging of HAMA hydrogels. (Scale bar, 10 μm.) (*D*) Schematic representation of a two-layered hydrogel assay of NPC migration toward NPCs, astrocytes, or neurons. (*E*) Representative images of NPC migration induced by NPCs, astrocytes, or neurons for indicated times. Dotted lines identify the farthest cell of each type; the distance between red and green dotted lines was considered the maximum migration distance. (Scale bar, 200 μm.) (*F*) Quantification of maximum migration distance induced by NPCs, astrocytes, or neurons (see *Materials and Methods*). Bars represent means; *P* < 0.05, and **P* < 0.01; n = 3. (*G*) Time-lapse images of NPC migration induced by astrocytes for 8 h. (Scale bar, 200 μm.) (*H*) Representative images of NPC migration induced by astrocytes for 1.5 d. Alexa647-labeled HAMA identifies the top layer. (Scale bar, 200 μm.)
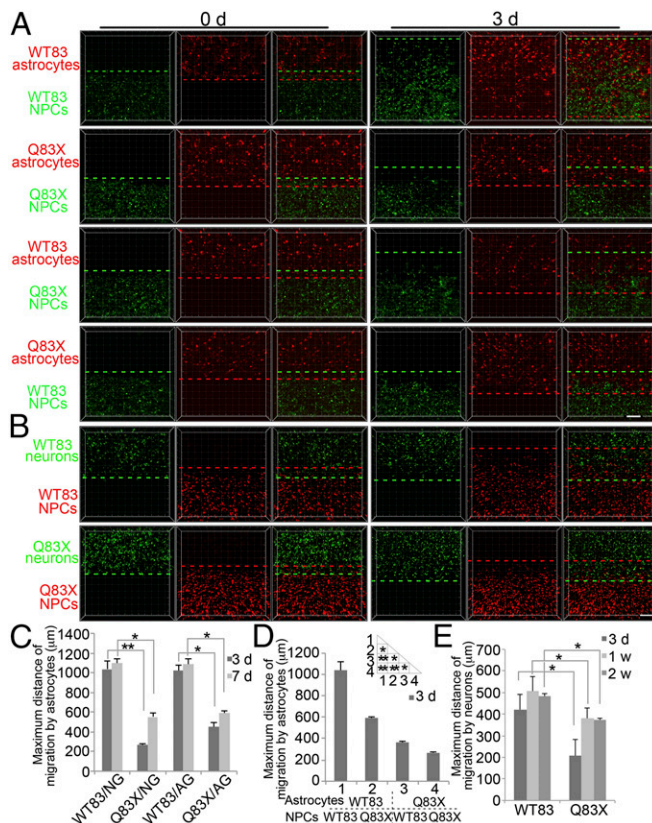
**Fig. 2.** Defective migration of Q83X NPCs toward astrocytes or neurons. (*A*) Representative microscopy images of WT83 and Q83X NPC migration induced by WT83 or Q83X astrocytes for indicated times. (Scale bar, 200 μm.) (*B*) Representative microscopy images of WT83 and Q83X NPC migration toward neurons for indicated times. (Scale bar, 200 μm.) (*C*) Quantification of maximum WT83 or Q83X NPC migration distance induced by WT83 or Q83X astrocytes in NG and AG medium (see *Materials and Methods*). Bars represent means; *$P < 0.05$, and **$P < 0.01$; $n = 3$. (*D*) Quantification of maximum WT83 NPC migration distance induced by WT83 or Q83X astrocytes and maximum Q83X NPC migration distance induced by WT83 or Q83X astrocytes in AG medium. Bars represent means; *$P < 0.05$, and **$P < 0.01$; $n = 3$. (*E*) Quantification of maximum migration distance toward neurons. Bars represent means; *$P < 0.05$; $n = 3$.

WT83 astrocytes was still retarded ~40% comparing to WT83 NPCs migration toward WT83 astrocytes, indicating intrinsic defect of Q83X NPCs migration itself, whereas WT83 NPC migration toward Q83X astrocytes was also ~55% retarded comparing to WT83 NPC migration toward WT83 astrocytes, indicating defect of Q83X astrocytes chemoattraction (Fig. 2 *A* and *D*). Thus, the phenotype appears to reflect both slower intrinsic migratory ability of Q83X NPCs and impaired chemoattraction by Q83X astrocytes. We further evaluated WT83 and Q83X NPC migration induced by neurons. Q83X NPC migration toward neurons was also retarded compared with WT83 NPCs (Fig. 2 *B* and *E*). Taken together, RTT NPCs carrying the Q83X variant of MeCP2 migrate shorter distances toward either astrocytes or neurons.

To rule out the influence of genetic factors besides the MeCP2 Q83X mutation as a cause of this phenotype, we used isogenic stem cells carrying a frame-shift mutation in the *MECP2* gene in a human embryonic stem cell (hESC) line (hESC–MeCP2 mutation). Similar migration assays using NPCs derived from these cells validated the defect in migration toward both astrocytes (Fig. S2 *A* and *E*) and neurons (Fig. S2 *C* and *F*). Additionally, we rescued a patient cell line with an early stop codon mutation (Q83X), restoring MeCP2 protein levels to normal (rQ83X). The defects in

migration toward both astrocytes (Fig. S2 *B* and *E*) and neurons (Fig. S2 *D* and *F*) were rescued when MeCP2 was restored in the cells (rQ83X). These results suggest that MeCP2 mutations impair cell-induced migration in 3D hydrogels.

To further confirm the migration defects caused by dysfunction of MeCP2, we repeated the 3D migration assay with NPCs derived from another male RTT patient (N126I) and his non-affected father's iPSC lines. Migration was examined in two-layer hydrogels containing sorted GFAP::tdTomato-positive astrocytes in the top layer and CMV::GFP-positive NPCs in the bottom layer. Similar migration defect due to both slower intrinsic migratory ability of N126I NPCs and impaired chemoattraction by N126I astrocytes was found (Fig. S3 *A* and *C*). We further evaluated WT126 and N126I NPC migration induced by neurons. N126I NPC migration toward neurons was also retarded compared with WT126 NPCs (Fig. S3 *B* and *D*). Taken together, RTT NPCs carrying the N126I variant of MeCP2 mutation migrate shorter distances toward either astrocytes or neurons.

**Three-Dimensional Hydrogel Culture Accelerates Neuronal Differentiation of Human iPSC-Derived NPCs.** As an initial step toward investigating RTT pathophysiology, we generated mature neurons from human iPSC-derived NPCs in our 3D culture system. NPCs were infected with lentivirus expressing GFP from the neuron-specific synapsin-1 (Syn) promoter, and differentiation was followed by monitoring GFP fluorescence. Control iPSC-derived Syn::GFP NPCs (WT83) expressing Nestin, Sox2, Sox1, and PAX6 (Fig. S1 *A* and *B*) were seeded in 3D hydrogels. Expression of GFP, indicating neuronal differentiation, was detectable within only 2 d (Fig. 3*A*). After 1 wk of culture in the hydrogel, neurite outgrowth from NPCs was already clearly visible, and neurites > 100 μm were apparent throughout the thickness of the hydrogel by week two (Fig. 3*A*). These cells were positive for neuronal markers such as Tuj1 and microtubule-associated protein 2 (Map2). Moreover, we also observed synapsin puncta outlining Map2-positive neurites (Fig. 3*B*). Compared with 2D culture, the density of syn1-positive puncta in 3D culture was significantly higher after 3 wk culture and was even more significant after 6 wk culture (Fig. 3*C*). To further confirm formation of synapses, we examined ultrastructure. Electron microscopy revealed typical synaptic vesicles and postsynaptic densities after 3 wk of differentiation in 3D hydrogels but only large clear vesicles at the same time in 2D culture. Only after 6 wk of differentiation in 2D culture did the postsynaptic densities appear. The density of synapses was significantly higher in 3D culture compared with 2D culture after both 3 wk and 6 wk of differentiation (Fig. 3*D*).

To examine whether 3D differentiated neurons were functionally mature, we transferred them to glass slides by digesting hydrogels containing NPCs expressing Syn::GFP and differentiated for 3 wk using hyaluronidase (2,000 units per milliliter) overnight. After 4 d of culture on slides, electrophysiological activity of GFP-positive cells was examined. Predigestion of 3D hydrogel is for recording and comparison with 2D differentiated neurons. The 2D differentiated neurons were also treated with hyaluronidase. In response to steps of depolarizing current, only neurons differentiated in 3D hydrogels but not in 2D culture for 3 wk fired trains of action potentials (Fig. 3*E*). Further, whole-cell voltage clamp recordings performed before and after application of 1 μM tetrodotoxin revealed functional voltage-activated sodium and potassium channels in 3D differentiated cells, but not in 2D culture, indicating fast maturation of 3D cultured cells (Fig. 3 *F* and *G*). In addition, we detected whether 3D differentiated neurons expressed functional glutamate and GABA receptors. Bath application of the neurotransmitter glutamate (100 μM) transiently induced an inward current, and these events were blocked by 20 μM 2,3-dihydroxy-6-nitro-7-sulfamoyl-benzo[f]quinoxaline-2,3-dione (NBQX) and 50 μM D-aminophosphonovalerate (APV), indicating the presence of functional glutamate receptors (Fig. 3*H*). Transient currents were also observed following 10 μM γ-aminobutyric acid (GABA) bath
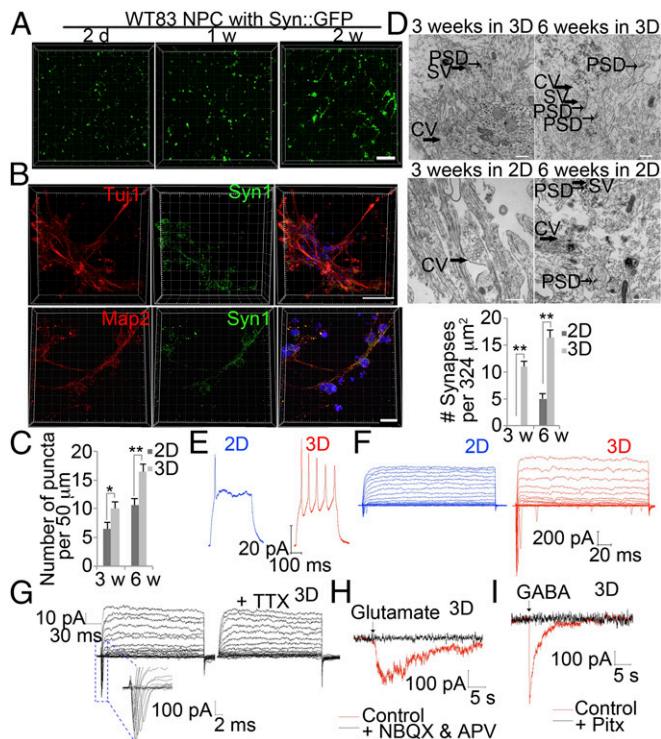
**Fig. 3.** Rapid maturation of human iPSC-derived neurons in 3D hydrogels. (*A*) Representative images of human iPSC-derived NPCs infected with Syn::GFP lentivirus after neuronal differentiation for indicated times in 3D hydrogels. (Scale bar, 200 μm.) (*B*) Representative images of human iPSC-derived neurons stained for Tuj1 or Map2 (red), Syn1 (green), and DAPI (blue) in 3D hydrogel. (Scale bar, 60 μm.) (*C*) Quantification of Syn1 puncta on Map2 neurites. Bars represent means of 50 neurons per condition; *$P < 0.05$, and **$P < 0.01$; $n = 3$. (*D*) Representative images of ultrastructural investigation of synaptogenesis by transmission electron microscopy in control NPCs differentiated in 3D or 2D system at indicated times. CV, large clear vesicle; SV, synaptic vesicle. Quantification of numbers of synapses in control NPCs differentiated in 3D or 2D system at indicated times. Bars represent means; **$P < 0.01$ by; $n = 3$. (Scale bar, 500 nm.) (*E*) Representative whole-cell current clamp recordings of human iPSC-derived neurons after 3 wk differentiation in 3D or 2D system. Spiking activity was examined following current injection. (*F*) Representative voltage clamp recording of a 3D or 2D cultured neuron held at −75 mV and then stepped to a series of voltages (−80 to +20 mV) in 5-mV increments. (*G*) Representative voltage clamp recording of a 3D cultured neuron before and after application of TTX. TTX, 1 μM tetrodotoxin. (*H*) Response to glutamate in the presence and absence of the glutamate receptor blockers 20 μM NBQX and 50 μM APV. (*I*) Response to GABA in the presence and absence of 50 μM picrotoxin (Pitx).

application, indicating the presence of functional GABA receptors, as these events were blocked by 50 μM picrotoxin (Fig. 3*I*). All these results suggest that NPC-derived neurons differentiated in 3D hydrogels for only 3 wk are functionally mature.

We further compared neuronal differentiation of Syn::GFP-expressing NPCs cultured either in 2D adherent culture or 3D hydrogels. By real-time PCR, the NPC marker Nestin was dramatically down-regulated in 3D cultured but not in 2D cultured cells, whereas neuronal markers, such as Syn1, vGlut1, CTIP2, and Map2 were elevated in both. However, mRNA expression of these neuronal markers in 3D cultured cells was significantly greater than that in 2D culture (Fig. S4*A*). Consistently, Syn promoter-driven GFP expression in 3D culture was also higher than in 2D culture (Fig. S4*B*), indicating greater neuronal differentiation.

To examine the proportion of NPCs that differentiate into neurons vs. astrocytes in 3D and 2D culture, we infected iPSC-derived NPCs with both lentiviral Syn::GFP and GFAP::tdTomato

(GFAP is an astrocyte marker). Although, in 2D culture, 10% of cells were GFAP-positive at 2 wk differentiation, few GFAP-positive cells were detected in 3D culture at this time point. At 5 wk, 2D cultures contained 26% GFAP-positive cells versus only 3.5% in 3D culture (Fig. S4 *C* and *D*). Further, a greater proportion of 3D than 2D cultured cells were double-negative for CD44 and CD184 (85% vs. 63%; Fig. S4*E*), cell surface markers used to isolate neurons derived from human pluripotent stem cells (18). These results show that differentiation of iPSC-derived NPCs in 3D hydrogels favors neuronal over glial differentiation and accelerates maturation of neurons compared with 2D culture.

Next, we directly tested whether there was any bias for differentiation into specific neuronal subtypes. In our 3D system, neurons were cultured in NG medium, which is widely used for differentiation of human cortical neurons (1, 22). Thus, we used TBR1 and vGluT1 to determine the proportions of cortical excitatory neurons, GABA and GAD1/GAD67 (the GABA synthetic enzyme) for GABAergic inhibitory neurons, CTIP2 (also known as BCL11B) for layer V/VI neuron, and TH1 for dopaminergic neuron (23) (Fig. S5). Most importantly, there was no significant difference in subtype populations between 3D cultured and 2D cultured neurons (Fig. S4*F*).

Hydrogel scaffold mechanical properties and presentation of biochemical cues can simulate the in vivo environment of the brain (24). Most importantly, the defined elastic modulus range of our HAMA hydrogels is consistent with native neural microenvironments (50–250 Pa), which is important for directing neural survival and axonal outgrowth (25, 26). We carefully tuned the mechanics of our system to accurately represent the in vivo condition. For example, we expected that scaffold elasticity would influence the extent of neurite outgrowth for differentiating NPCs. We tested our hypothesis by tracking extension length as a function of varied elastic moduli over a biologically relevant range. As shown in Fig. 1*B*, altering the UVA irradiation time at 60 s, 90 s, or 120 s resulted in HAMA hydrogel matrices with elastic moduli of 130 Pa, 260 Pa, and 520 Pa, respectively. Neurons differentiated within more elastic 130-Pa scaffolds exhibited greater neurite outgrowth compared with those differentiated within less elastic, 260 Pa and 520 Pa, scaffolds (Fig. S6). These data illustrate our effort to identify and optimize scaffold conditions critical to our 3D neural model of migration, differentiation, and neurite outgrowth.

Cell adhesion, spreading, and locomotion on 2D substrates is inversely proportional to substrate elasticity for a wide range of elastic moduli. Native ECM elasticity is tissue-dependent; however, cells are typically rounded, minimally adhesive, growth-arrested and prone to apoptosis when grown on soft 2D matrices (27). For this study, we designed a scaffold to mimic native mechanical and biochemical properties of the developing CNS (25, 26). Not surprisingly, our initial efforts to cultivate NPCs and astrocytes on 2D soft material substrates were unsuccessful. Encapsulating and absorbing laminin into 2D HAMA hydrogels failed to promote attachment and spreading. Instead, NPCs quickly aggregated and detached as spheres (Fig. S7 *A* and *B*). It has been reported that cell adhesion peptides and proteins engineered into hydrogels promote neuronal differentiation and outgrowth (24, 28). Therefore, we covalently cross-linked potent integrin-binding adhesion ligands into the hydrogel surface, specifically Arg-Gly-Asp (RGD), Tyr-Ile-Gly-Ser-Arg (YIGSR), and Ile-Lys-Val-Ala-Val (IKVAV), to compliment the innate CD44-binding property of hyaluronic acid. Acryl-PEG3400-GRGD, Acryl-PEG3400-GYIGSR, and Acryl-PEG3400-ASIKVAVS were custom-ordered (21st Century Biochemical and Laysan Bio). We tested cell adhesion on ligand-functionalized 2D HAMA hydrogels 12 h after initial seeding. RGD peptide, but not YIGSR or IKVAV, promoted initial NPC attachment (Fig. S7 *A* and *B*). Further, we optimized the RGD concentration-dependent initial adhesion and spreading. Despite initial NPC attachment, NPCs only adhered to "optimized" RGD HAMA surfaces for 2 d before

aggregating, and ultimately detached after 3 d (Fig. S7C). Within the initial 2-d period, using time-lapse fluorescence microscopy, we observed no NPC migration toward discretely cocultured astrocytes on 2D RGD HAMA substrates (Fig. S7 D and F). Identical functionalization in 3D RGD HAMA scaffolds had no adverse effect on encapsulated astrocyte-induced NPC migration over the same time period (Fig. S7 E and F).

### Reduced Neurite Outgrowth and Synapse Number in RTT Neurons in 3D Hydrogel.

Reduced dendritic arborization has been observed both in RTT patient cortex (29) and in some MeCP2 mutant mice (30), but whether this results from reduced branching during development or from a failure of dendrite maintenance remains unclear. Similarly, disorganization of axons within cortical layers has been observed both in patients and animal models (31). The underlying mechanism behind dendritic arborization could be most easily studied in vitro using human neurons generated from patient iPSCs. We therefore compared neurite outgrowth between MeCP2 Q83X neurons derived from RTT patient iPSCs and control neurons derived from a parent's iPSCs in our 3D hydrogel system. Neurite outgrowth in Q83X neurons was much slower, producing much shorter neurites than WT83 (Fig. 4 A−C). The difference became apparent at as early as day three and remained significant throughout 42 d of culture (Fig. 4 A−C). To further confirm this difference, we used immunostaining to detect Syn-positive puncta along Map2-positive neurites. Syn puncta were far less dense in Q83X neurons than controls (Fig. 4 D and E), confirming our prior findings in 2D culture (1). To further study the maturation defect, we recorded spontaneous excitatory postsynaptic currents (sEPSCs) as a way of measuring intercellular connectivity and network formation (Fig. 4F). Cumulative probability plots of amplitudes and interevent intervals of spontaneous postsynaptic currents revealed that RTT neurons have a significant decrease in frequency compared with WT neurons (Fig. 4F). Defective neurite outgrowth (Fig. S8 A and C) and a lower density of Syn puncta in Q83X neurons was confirmed using neurons generated from isogenic cell-derived NPCs (Fig. S8 B and D).

To further confirm the reduced neurite outgrowth and synapse number caused by dysfunction of MeCP2, we used the NPCs derived from another male RTT patient (N126I) and his non-affected father's iPSC lines. Neurite outgrowth in N126I neurons was much slower, producing much shorter neurites than WT126 (Fig. S9 A and C). Next, we used immunostaining to detect Syn-positive puncta along Map2-positive neurites. Syn puncta were far less dense in N126I neurons than controls (Fig. S9 B and D). Taken together, our data confirm previous observations of reduced neurite outgrowth and synapse number in RTT neurons.

### Discussion

Migration of human-derived NPCs has been examined in 3D hydrogels by transplantation into adult rat brains (32), but no method has yet been developed to study 3D migration of human-derived NPCs in vitro. Although NPC migration may be assessed using chemotaxis chambers, such assays may not accurately reflect in vivo differences, as cells can also migrate through aqueous media across membranes rather than specifically along a 3D matrix. The most common in vitro approach for studying 3D migration, coculture with tissue pieces or heterogeneous cell aggregates expressing secreted neurotrophins, has only been applied to tissue explants (33). In this study, we describe a previously unidentified 3D system for manipulating neuronal migration in vitro. This system provides better spatial control and may be more suited to observing single cells than tissue explant cultures.

Rapid generation of neurons in 3D hydrogels could result from several mechanisms. (i) Close matching of the physical properties of the brain [the elastic modus of soft, neurite-supportive hydrogels (100 Pa) is similar to that of brain tissue] (26) may accelerate
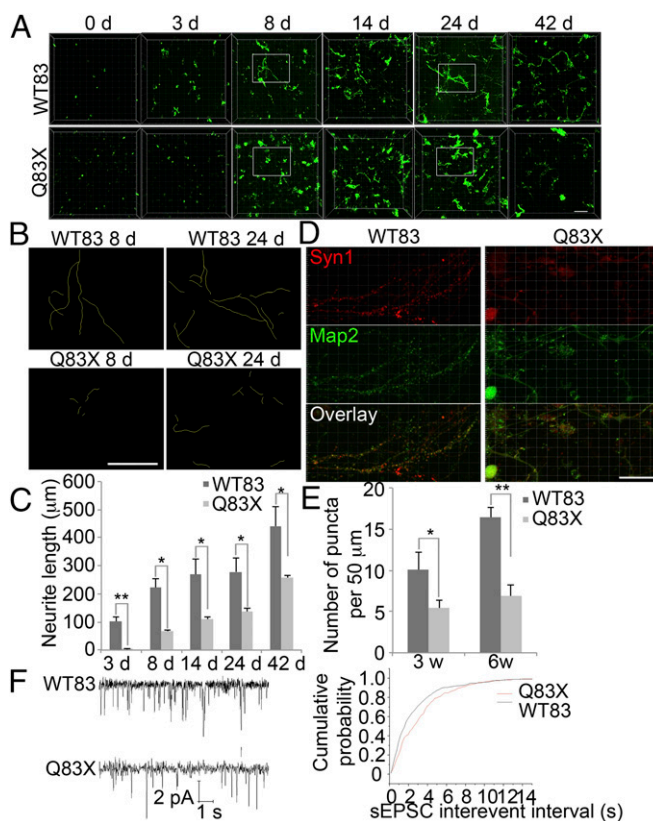


**Fig. 4.** Defective neurite outgrowth and synapse formation in Q83X neurons in 3D hydrogel. (A) Representative images of WT83 and Q83X cells after neuronal differentiation in 3D hydrogel at different times. (Scale bar, 200 μm.) (B) Neuronal tracing comparing WT83 and Q83X neurons at day 8 and day 24 after differentiation. (C) Quantification of neurite length. Bars represent means of 50 neurons per condition; *$P < 0.05$, and **$P < 0.01$; $n = 3$. (D) Representative images of WT83 and Q83X neurons showing Syn1 puncta on Map2-positive neurites. (Scale bar, 20 μm.) (E) Quantification of Syn1 puncta on Map2 neurites. Bars represent means of 50 neurons per condition; *$P < 0.05$, and **$P < 0.01$; $n = 3$. (F) Spontaneous currents recording of WT83 and Q83X neurons. Cumulative probability plot of interevent intervals ($P < 0.05$) of sEPSCs from groups of WT83 (black) and Q83X (red) cells shown; $n = 5$.

differentiation. Materials whose mechanical properties closely mimic those of the in vivo ECM of a particular soft tissue have been shown to promote differentiation of progenitor cells into the mature phenotypes inherent to that tissue (34). (ii) The 3D scaffold may allow generation of mechanical force by NPCs in response to their environment (11). (iii) The 3D environment provides a high surface area for growth and migration (35), which can be tuned to support other cell behaviors, such as differentiation or maturation. In vivo-like cell−cell interactions may lead to more realistic gene expression and cellular behavior.

We synthesized cross-linkable HA with the intention to exploit the innate bioactive properties of this high molecular weight glycosaminoglycan naturally abundant in the brain. HA plays a prominent structural role in brain ECM and is upregulated along NPC migratory routes in the developing brain. Many nonneuronal neural cell types express HA receptor CD44, including NPCs and astrocytes (36). Notably, momentary cellular focal adhesions are less stable during HA/CD44 ligation in HA matrices alone compared with α/β integrin-mediated ligation in the added presence of potent ECM ligands such as RGD peptide (37). We encapsulated laminin protein, another key neural ECM component that comprises such ligands, within our HAMA scaffolds to support viability of neural cells. Laminin especially

ENGINEERING

promoted neurite dynamics in differentiating neurons, which cease to express CD44. However, because we did not covalently bind laminin to the matrix, it likely did not significantly contribute to anchorage-dependent NPC locomotion. Native neural ECM varies in character and distribution, with unique molecular structure surrounding a wide variety of neurons. ECM affects both the differentiation efficiency and the derived cell function of developing neural cells (38). Physically entrapping ECM proteins, such as collagen, laminin, or fibronectin, in the synthetic hydrogels has been shown to promote NPC differentiation (39). Although we demonstrated that HAMA hydrogels with laminin only are sufficient to induce NPC differentiation, additional cell adhesion cues might further enhance biomimicry in our 3D system.

In summary, our hydrogel-based assay of neural migration reveals a defect in NPCs derived from an RTT patient's iPSCs. Further, this hydrogel system facilitates neuronal differentiation and maturation, reducing the time needed to generate functional neurons from over 6 wk to just 3 wk. Using this method to examine migration and differentiation of NPCs derived from patient iPSCs should yield more reliable results than other approaches, as cells move through a soft matrix rather than across a hard surface or through a membrane. Further, it allows exploration of responses to various cell types and biochemical cues without the need for neurosphere culture, which is time-consuming and often inefficient. This system could also be used to screen drug candidates for their ability to restore disease-associated defects in migration or other phenotypes more appropriately studied in 3D systems.

## Materials and Methods

For migration, two-layered hydrogels were swollen in medium for 12 h and termed as "0 day." Live-cell images of the region where the two layers meet were acquired using Olympus confocal microscope. Generation and use of human iPSCs and their derived cells were approved by the University of California, San Diego human research protection program committee meeting under the IRB/ESCRO protocol 141223ZF. All participants gave informed consent to the procedures. All experiments using human materials have been conducted according to the principles expressed in the Declaration of Helsinki. Number of clones from iPSCs used in each experiment in this study is listed in Table S1. Primer sequences for real-time PCR are listed in Table S2. For more materials and methods, please see SI Materials and Methods.

1. Marchetto MCN, et al. (2010) A model for neural development and treatment of Rett syndrome using human induced pluripotent stem cells. *Cell* 143(4):527–539.
2. Deutsch SI, Burket JA, Katz E (2010) Does subtle disturbance of neuronal migration contribute to schizophrenia and other neurodevelopmental disorders? Potential genetic mechanisms with possible treatment implications. *Eur Neuropsychopharmacol* 20(5):281–287.
3. Khetan S, et al. (2013) Degradation-mediated cellular traction directs stem cell fate in covalently crosslinked three-dimensional hydrogels. *Nat Mater* 12(5):458–465.
4. Zorlutuna P, et al. (2012) Microfabricated biomaterials for engineering 3D tissues. *Adv Mater* 24(14):1782–1804.
5. Otsuji TG, et al. (2014) A 3D sphere culture system containing functional polymers for large-scale human pluripotent stem cell production. *Stem Cell Rep* 2(5):734–745.
6. Dvir T, Timko BP, Kohane DS, Langer R (2011) Nanotechnological strategies for engineering complex tissues. *Nat Nanotechnol* 6(1):13–22.
7. DeForest CA, Tirrell DA (2015) A photoreversible protein-patterning approach for guiding stem cell fate in three-dimensional gels. *Nat Mater* 14(5):523–531.
8. Choi HK, Won L, Heller A (1993) Dopaminergic neurons grown in three-dimensional reaggregate culture for periods of up to one year. *J Neurosci Methods* 46(3):233–244.
9. Lampe KJ, Antaris AL, Heilshorn SC (2013) Design of three-dimensional engineered protein hydrogels for tailored control of neurite growth. *Acta Biomater* 9(3): 5590–5599.
10. Leipzig ND, Shoichet MS (2009) The effect of substrate stiffness on adult neural stem cell behavior. *Biomaterials* 30(36):6867–6878.
11. Seidlits SK, et al. (2010) The effects of hyaluronic acid hydrogels with tunable mechanical properties on neural progenitor cell differentiation. *Biomaterials* 31(14): 3930–3940.
12. Paşca AM, et al. (2015) Functional cortical neurons and astrocytes from human pluripotent stem cells in 3D culture. *Nat Methods* 12(7):671–678.
13. Choi SH, et al. (2014) A three-dimensional human neural cell culture model of Alzheimer's disease. *Nature* 515(7526):274–278.
14. Amir RE, et al. (1999) Rett syndrome is caused by mutations in X-linked MeCP2, encoding methyl-CpG-binding protein 2. *Nat Genet* 23(2):185–188.
15. Chen WG, et al. (2003) Derepression of BDNF transcription involves calcium-dependent phosphorylation of MeCP2. *Science* 302(5646):885–889.
16. Karpiak JV, Ner Y, Almutairi A (2012) Density gradient multilayer polymerization for creating complex tissue. *Adv Mater* 24(11):1466–1470.
17. Mason HA, Ito S, Corfas G (2001) Extracellular signals that regulate the tangential migration of olfactory bulb neuronal precursors: Inducers, inhibitors, and repellents. *J Neurosci* 21(19):7654–7663.
18. Yuan SH, et al. (2011) Cell-surface marker signatures for the isolation of neural stem cells, glia and neurons derived from human pluripotent stem cells. *PLoS One* 6(3): e17540.
19. Scala E, et al. (2005) CDKL5/STK9 is mutated in Rett syndrome variant with infantile spasms. *J Med Genet* 42(2):103–107.
20. Chen Q, et al. (2010) CDKL5, a protein associated with Rett syndrome, regulates neuronal morphogenesis via Rac1 signaling. *J Neurosci* 30(38):12777–12786.
21. Neul JL, Zoghbi HY (2004) Rett syndrome: A prototypical neurodevelopmental disorder. *Neuroscientist* 10(2):118–128.
22. Griesi-Oliveira K, et al. (2015) Modeling non-syndromic autism and the impact of TRPC6 disruption in human neurons. *Mol Psychiatry* 20(11):1350–1365.
23. Mariani J, et al. (2015) FOXG1-dependent dysregulation of GABA/glutamate neuron differentiation in autism spectrum disorders. *Cell* 162(2):375–390.
24. McKinnon DD, Kloxin AM, Anseth KS (2013) Synthetic hydrogel platform for three-dimensional culture of embryonic stem cell-derived motor neurons. *Biomater Sci-Uk* 1(5):460–469.
25. Lu YB, et al. (2006) Viscoelastic properties of individual glial cells and neurons in the CNS. *Proc Natl Acad Sci USA* 103(47):17759–17764.
26. Flanagan LA, Ju YE, Marg B, Osterfield M, Janmey PA (2002) Neurite branching on deformable substrates. *Neuroreport* 13(18):2411–2415.
27. Wells RG (2008) The role of matrix stiffness in regulating cell behavior. *Hepatology* 47(4):1394–1400.
28. Silva GA, et al. (2004) Selective differentiation of neural progenitor cells by high-epitope density nanofibers. *Science* 303(5662):1352–1355.
29. Armstrong D, Dunn JK, Antalffy B, Trivedi R (1995) Selective dendritic alterations in the cortex of Rett syndrome. *J Neuropathol Exp Neurol* 54(2):195–201.
30. Stuss DP, Boyd JD, Levin DB, Delaney KR (2012) MeCP2 mutation results in compartment-specific reductions in dendritic branching and spine density in layer 5 motor cortical neurons of YFP-H mice. *PLoS One* 7(3):e31896.
31. Belichenko PV, et al. (2009) Widespread changes in dendritic and axonal morphology in MeCP2-mutant mouse models of Rett syndrome: Evidence for disruption of neuronal networks. *J Comp Neurol* 514(3):240–258.
32. Englund U, Björklund A, Wictorin K (2002) Migration patterns and phenotypic differentiation of long-term expanded human neural progenitor cells after transplantation into the adult rat brain. *Brain Res Dev Brain Res* 134(1-2):123–141.
33. Gil V, del Río JA (2012) Analysis of axonal growth and cell migration in 3D hydrogel cultures of embryonic mouse CNS tissue. *Nat Protoc* 7(2):268–280.
34. Yang C, Tibbitt MW, Basta L, Anseth KS (2014) Mechanical memory and dosing influence stem cell fate. *Nat Mater* 13(6):645–652.
35. Schultz KM, Kyburz KA, Anseth KS (2015) Measuring dynamic cell-material interactions and remodeling during 3D human mesenchymal stem cell migration in hydrogels. *Proc Natl Acad Sci USA* 112(29):E3757–E3764.
36. Lindwall C, Olsson M, Osman AM, Kuhn HG, Curtis MA (2013) Selective expression of hyaluronan and receptor for hyaluronan mediated motility (Rhamm) in the adult mouse subventricular zone and rostral migratory stream and in ischemic cortex. *Brain Res* 1503:62–77.
37. Kim Y, Kumar S (2014) CD44-mediated adhesion to hyaluronic acid contributes to mechanosensing and invasive motility. *Mol Cancer Res* 12(10):1416–1429.
38. Ma W, et al. (2008) Cell-extracellular matrix interactions regulate neural differentiation of human embryonic stem cells. *BMC Dev Biol* 8:90.
39. Blewitt MJ, Willits RK (2007) The effect of soluble peptide sequences on neurite extension on 2D collagen substrates and within 3D collagen gels. *Ann Biomed Eng* 35(12):2159–2167.
40. Fairbanks BD, Schwartz MP, Bowman CN, Anseth KS (2009) Photoinitiated polymerization of PEG-diacrylate with lithium phenyl-2,4,6-trimethylbenzoylphosphinate: Polymerization rate and cytocompatibility. *Biomaterials* 30(35):6702–6707.
41. Bamji SX, et al. (2003) Role of beta-catenin in synaptic vesicle localization and presynaptic assembly. *Neuron* 40(4):719–731.